HOKKAIDO UNIVERSITY

| | |
|---|---|
| Title | Quantitative analysis of condensation/decondensation status of pDNA in the nuclear sub-domains by QD-FRET |
| Author(s) | Shaheen, Sharif M.; Akita, Hidetaka; Yamashita, Atsushi et al. |
| Citation | Nucleic Acids Research, 39(7), e48<br>https://doi.org/10.1093/nar/gkq1327 |
| Issue Date | 2011-04 |
| Doc URL | https://hdl.handle.net/2115/45389 |
| Type | journal article |
| File Information | NAR39-7_e48.pdf |




Hokkaido University Collection of Scholarly and Academic Papers : HUSCAP

*Published online 1 February 2011*

*Nucleic Acids Research, 2011, Vol. 39, No. 7* ***e48***
*doi:10.1093/nar/gkq1327*

# Quantitative analysis of condensation/decondensation status of pDNA in the nuclear sub-domains by QD-FRET

**Sharif M. Shaheen[1], Hidetaka Akita[1], Atsushi Yamashita[2], Ryo Katoono[2], Nobuhiko Yui[2,*], Vasudevanpillai Biju[3], Mitsuru Ishikawa[3] and Hideyoshi Harashima[1,*]**

[1]Laboratory for Molecular Design of Pharmaceutics, Faculty of Pharmaceutical Sciences, Hokkaido University, Kita-12, Nishi-6, Kita-ku, Sapporo 060-0812, [2]School of Materials Science, Japan Advanced Institute of Science and Technology, 1-1 Asahidai, Nomi, Ishikawa 923-1292 and [3]Nanobioanalysis Team, Health Technology Research Center, National Institute of Advanced Industrial Science and Technology, 2217-14 Hayashi-cho, Takamatsu, Kagawa 761-0395, Japan

Received April 23, 2010; Revised November 25, 2010; Accepted December 14, 2010

## ABSTRACT

**Recent studies indicate that controlling the nuclear decondensation and intra-nuclear localization of plasmid DNA (pDNA) would result in an increased transfection efficiency. In the present study, we established a technology for imaging the nuclear condensation/decondensation status of pDNA in nuclear subdomains using fluorescence resonance energy transfer (FRET) between quantum dot (QD)-labeled pDNA as donor, and rhodamine-labeled polycations as acceptor. The FRET-occurring pDNA/polycation particle was encapsulated in a nuclear delivery system; a tetra-lamellar multifunctional envelope-type nano device (T-MEND), designed to overcome the endosomal membrane and nuclear membrane via step-wise fusion. Nuclear subdomains (i.e. heterochromatin and euchromatin) were distinguished by Hoechst33342 staining. Thereafter, Z-series of confocal images were captured by confocal laser scanning microscopy. pDNA in condensation/decondensation status in heterochromatin or euchromatin were quantified based on the pixel area of the signals derived from the QD and rhodamine. The results obtained indicate that modulation of the supra-molecular structure of polyrotaxane (DMAE-ss-PRX), a condenser that is cleaved in a reductive environment, conferred euchromatin-preferred decondensation. This represents the first demonstration of the successful control of condensation/decondensation in specific nuclear sub-domain via the use of an artificial DNA condenser.**

## INTRODUCTION

In post-genome era, gene therapy is one of the new-generation approaches for the cure of intractable diseases, which can complement the defective gene (1–3). Since viral gene carrier potentially has adverse effects such as oncogenicity (4) and inflammation (5), efficient non-viral carrier is highly desired. It is generally considered that transfection activity is rate limited by a variety of intracellular process such as endosomal escape and nuclear transfer (6). Recent quantitative comparison of intracellular trafficking of plasmid DNA (pDNA) and adenovirus collectively revealed that post-nuclear delivery processes (i.e. transcription and translation) are dominant rate-limiting processes for the 2- or 3-order of magnitude less transfection efficiency in non-viral vectors (7–9). Further mechanism-based studies clarified that pDNA transfected with lipoplex mainly exist as condensed form in the nucleus, which prevents it from the access to transcription factors (7). In contrast, adenovirus genomic DNA is efficiently released in the nucleus. Moreover, adenoviral genome DNA was specifically localized on the euchromatin region (7), where transcription activity is relatively active (10–13).

Herein, we established an imaging technology for visualizing and quantifying nuclear decondensation in specified nuclear sub-domains by means of fluorescence

*To whom correspondence should be addressed. Tel: +81 11 706 3919; Fax +81 11 706 4879; Email: harasima@pharm.hokudai.ac.jp
Correspondence may also be addressed to Nobuhiko Yui. Tel: +81 761 51 1640; Fax +81 761 51 1645; Email: yui@jaist.ac.jp

The authors wish it to be known that, in their opinion, the first two authors should be regarded as joint First Authors.

© The Author(s) 2011. Published by Oxford University Press.
This is an Open Access article distributed under the terms of the Creative Commons Attribution Non-Commercial License (http://creativecommons.org/licenses/by-nc/2.5), which permits unrestricted non-commercial use, distribution, and reproduction in any medium, provided the original work is properly cited.

Downloaded from nar.oxfordjournals.org at (D) Hokkaido U Med on May 9, 2011

resonance energy transfer (FRET) between quantum dot (QDs)-labeled pDNA as a donor, and rhodamine-labeled polycation as an acceptor.

FRET is a promising technique for monitoring decondensation processes in cells, that occurs between donor–acceptor dyes tagged on single DNA molecules (14), or between dyes separately tagged on pDNA and a carrier (15,16). Of note, an analysis of FRET in the nucleus indicated that pDNA transfected with linear polyethylenimine or histidylated polylysine are present in the nucleus in a condensed form (15). To explain gene expression in terms of intranuclear disposition, quantification of the condensation/decondensation status in more specified intranuclear regions is required. In the present study, we established a technique for quantifying pDNA in a condensed or decondensed form in heterochromatin and euchromatin. In this system, we used QD as a donor, since it has been successfully used as a probe for the analysis of intracellular trafficking of macromolecules, including DNA in the past (17,18). Although CdSe-QD has some cytotoxicity due to the release of cadmium ions under UV-radiation (19), fluorescent CdSe/ZnS nanocrystals have been reported to be ideal for the use in long-term, non-toxic imaging of nuclear targeting in living cells (20), since they show superior brightness and resistance to photobleaching, compared to organic fluorophores. These unique characteristics facilitate the identification of the nuclear localization of pDNA and avoid the risks associated with loss of DNA-derived signals by repeated excitation when Z-stack images are obtained. It is also noteworthy that the emission spectra of QDs can be easily modulated by changing the size of the QD, thus permitting spectral overlap to be optimized (21). The quantification of intracellular and intra-nuclear decondensation by monitoring FRET QD-labeled pDNA and acceptor-labeled polycations has been reported previously (22). In the present study, we advanced this analysis by one-step further, characterizing the nuclear sub-domain to which the DNA was routed.

For an evaluation of the nuclear dispositions in relation to the transgene expression, efficient nuclear delivery system is prerequisite. For this purpose, a pDNA/polycation core was encapsulated in multilayered lipid envelope-type nanoparticle was used, which we refer to as a tetra-lamellar multi-functional envelope-type nano device (T-MEND) (23). In this system, condensed DNA cores are coated with two nuclear membrane-fusogenic inner envelopes and two endosome-fusogenic outer envelopes, both of which are designed to overcome the endosomal membrane and nuclear membranes, respectively.

Using the present method, we were able to demonstrate the first successful control of a condensation/decondensation profile in the intra-nuclear sub-domain using a synthetic polycation, polyrotaxane (PRX), which possessed a necklace-like structure composed of dimethylaminoethyl-modified α-cyclodextrin; DMAE-α-CD) and a disulfide-introduced PEG chain (15). To render it bio-cleavable, the end of the PEG chain was capped via disulfide bonding (Figure 1a). The flexible movement of α-CDs along with the PEG thread facilitates electrostatic interactions between pDNA and PRX multivalently by avoiding spatial mismatching (24). Thus, the method is useful in investigating the mechanism of extensive gene expression, and in understanding the rate-limiting processes to be overcome for further gene expression from the point of view of intra-nuclear disposition.

## MATERIALS AND METHODS

### Materials

1.2-Dioleoyl sn-glycero-3-phosphatidylethanolamine (DOPE) was purchased from Avanti Polar lipids (Alabaster, AL, USA). Cardiolipin (CL) and phosphatidic acid (PA) were purchased form Sigma (St Louis, MO, USA). Protamine sulfate salmon mint was purchased from Calbiochem (Darmstadt, Germany). Plasmid DNA pCMV-luc encoding luciferase was prepared using an EndoFree Plasmid Mega Kit (Qiagen, Germany). Stearyl octaarginine (STR-R8) (25) and cholesteryl-GALA (26) was custom-synthesized by NeoMPS (NeoMPS Inc., San Diego, CA, USA). HeLa cells were obtained from the RIKEN Cell Bank (Tsukuba, Japan) and Health Science Research Resources Bank (Osaka, Japan), respectively. In this study, we used luciferase (GL3)-inserted plasmid DNA. To prepare the luciferase-encoding vector, an insert fragment encoding luciferase (GL3) was obtained by Hind III/Xba I digestion of the pGL3-basic vector (Promega, Madison, WI, USA), and ligated to the HindIII/Xba I digested site of pcDNA3.1 (Invitrogen, Carlsbad, CA, USA) as reported previously (8,27). QD-545 streptavidin was obtained from Invitrogen.

### Preparation of polyplexes of pcDNA 3.1-luc and polyrotaxanes

In order to prepare pDNA core particle with DMAE-ss-PRX, 100 µl of naked pDNA solution (0.1 µg/µl in 10 mM HEPES) was added to 100 µl of polycation solution as demonstrated previously (28). The concentration of the DMAE-ss-PRX ($C_p$) at charge ratios was calculated using the following equation:

$$\text{Charge ratio } (\pm) = \{C_p \times N_{DMAE}/MW_p\}/(C_D/MW_D),$$

where, $N_{DMAE}$ denote the number of DMAE (16 in 16DMAE-ss-PRX and 46 in 46DMAE-ss-PRX) residues in the polycation molecule. The charge ratio (±) denotes the ratio of number of positive charges derived from amino groups of DMAE-ss-PRX to that of negative charges on phosphate groups of DNA. $MW_P$ and $MW_D$ denote the molecular weight of the polycation (16DMAE-ss-PRX: 24600, 46DMAE-ss-PRX:29200) and one nucleotide (average: 308), respectively.

$C_D$ denotes the concentration of pDNA (0.1 µg/µl). In the present study, we prepared the condensed core at charge ratio of 5. In this condition, a 2.4 µl aliquot of pDNA (2.5 µg/µl) (0.1µg/µl final concentration) was mixed with a 9 µl aliquot of 10 mM of DMAE-units DMAE-ss-PRX (final concentration 1 mM of DMAE units). The diameter and zeta-potential of the T-MEND

Downloaded from nar.oxfordjournals.org at (D) Hokkaido U Med on May 9, 2011

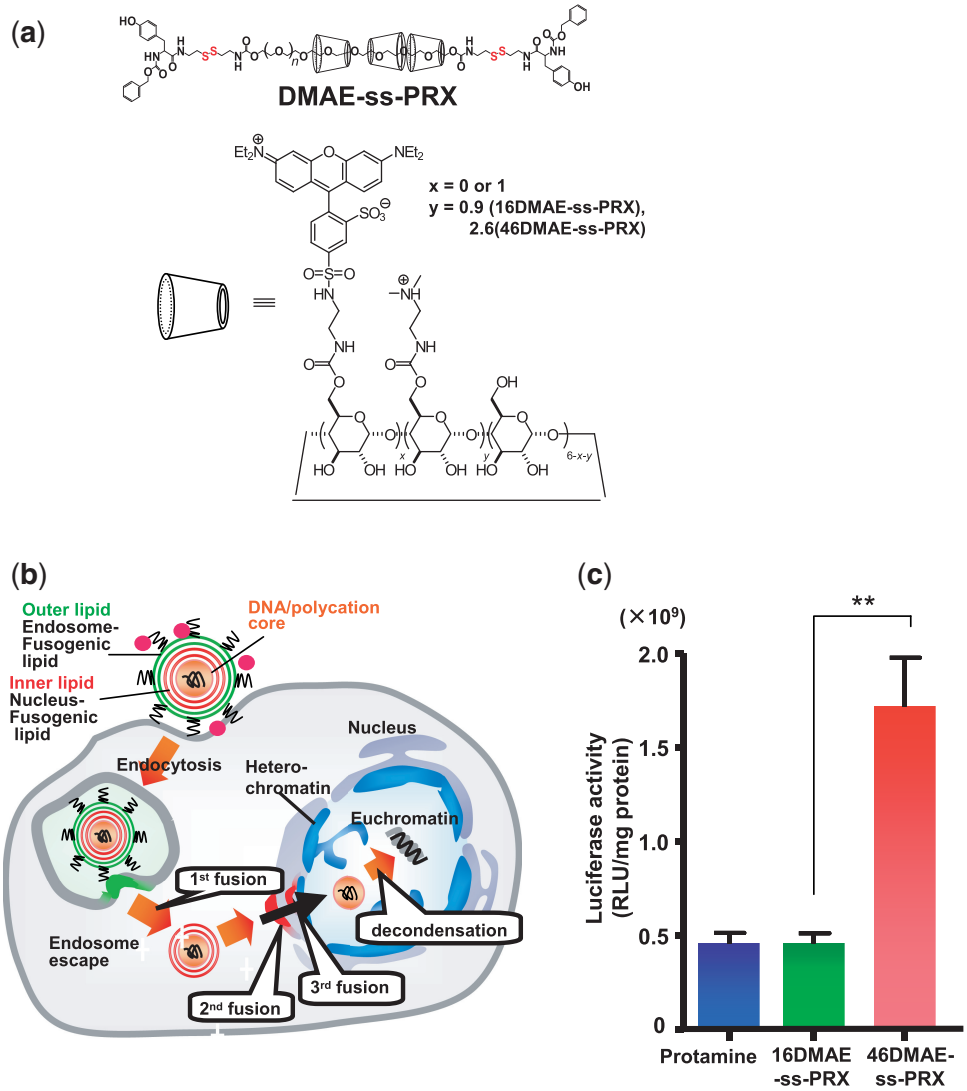



**Figure 1.** Schematic diagram illustrating technologies for intracellular trafficking and programed decondensation. (**a**) Structure of DMAE-ss-PRX and rhodamine-labeled DMAE-ss-PRX. It has an orientation, which resembles to a necklace-like structure composed of dimethylaminoethyl-modified α-cyclodextrin; DMAE-α-CD and a disulfide-introduced PEG chain. Moreover, the end of the PEG chain was capped via disulfide bonding. The number of threaded α-CDs and the molecular weight of PEG in the polyrotaxanes were 18 and 4000, respectively. (**b**) The strategy to deliver pDNA to the nucleus via a series of membrane fusions using T-MEND. pDNA is condensed with a polycation and then coated with a nucleus-fusogenic lipid membrane (inner) and an endosome-fusogenic lipid membrane (outer). The surface is modified with a high density of octaarginine (R8), which marks the liposomes for internalization into cells via macropinocytosis (40). During stepwise fusion, the pDNA/polycation core is released from the lipid envelope, which is advantageous for efficient transcription. (**c**) Transfection activity of T-MENDs encapsulating pDNA core particles formed with DMAE-ss-PRXs and protamine. HeLa cells were transfected with T-MENDs containing luciferase-encoding pDNA for 24 h. And thereafter transgene expression (luciferase activity) was performed as described in 'Materials and Methods' section.

were determined using an electrophoretic light-scattering spectrophotometer (Zetasizer; Malvern Instruments Ltd, Malvern, WR, UK). As a reference of gene transfection, pDNA was also condensed with protamine at charge ratio of 2.2 as described previously (27).

### Preparation of T-MEND

Lipid films composed of DOPE/CL = 5:5 (total lipid content: 0.55 mmol) were hydrated with 1 ml of 10 mM HEPES buffer (pH 7.4) for 10 min at room temperature. The hydrated lipid film was then sonicated using a probe-type sonicator (BRANSON Digital Sonifier-250; Danbury, CT, USA) with an amplitude of 25% for 10 min to form single unilamellar vesicles (SUVs1). Similarly, SUVs was prepared with DOPE with phosphatidic acid (PA) of 7:2 ratio (total lipid content: 0.55 mmol) and additional 1% mol of cholesterol-modified GALA peptide (SUVs2). Condensed DNA particles prepared above were mixed with SUVs1 at a ratio of 2:1 (v/v) to coat the condensed DNA particles with a double-lipid envelope as described previously (29,30). A stearylated octaarginine (STR-R8) solution (20% mol of total lipid) was added to the suspension of double-layered nuclear membrane-fusogenic particles. Then, this suspension of nuclear membrane-fusogenic particles was mixed

Downloaded from nar.oxfordjournals.org at (D) Hokkaido U Med on May 9, 2011

with endosome-fusogenic SUVs2 at a ratio of 1:2 (v/v) to generate particles with a double endosome-fusogenic envelope, which we refer to as T-MEND. Stearylated octaarginine (STR-R8) solution (10% mol of endosome-fusogenic lipid) was added to the suspension of T-MEND to modify the outer envelope with R8.

### Transfection studies

HeLa were maintained in Dulbecco's modified Eagle's medium (DMEM) supplemented with 10% fetal bovine serum at 37°C under an atmosphere with 5% $CO_2$. Cells were seeded onto 24-well plates at a density of $4 \times 10^4$ cells per well for 48 h. A 100 µl aliquot of T-MEND containing 0.4 µg DNA in serum-free DMEM (1.9 ml) was applied, and incubated for 3 h. Then, the culture media were replaced with a fresh medium containing a 6% serum, and additionally incubated for 21 h. For a luciferase assay, cells were washed with 0.5 ml of phosphate-buffered saline (PBS; pH 7.4). Reporter lysis buffer (0.2 ml) was then added to each well to lyse the cells. The cell suspension was next frozen by placing them in an −80°C freezer for 30 min, and thawed, followed by centrifugation at 15 000 rpm for 2 min. The relative light units (RLU) were measured using a luminometer (Bio-instrument ATTO Luminescencer AB-2200, Japan), and normalized to the protein content using the bicinchoninic acid (BCA) protein assay (Bio-Rad).

### FRET optimization

pDNA was labeled with a Mirus Label IT® CX-biotin nucleic acid labeling kit (Mirus Corp., Madison, WI, USA) with minor modifications. Shortly, the pDNA was labeled in optimized buffer supplied in the kit, but the Label IT solution was mixed at a 1/10 concentration of the manufacturer's recommended protocol of a Mirus Label IT® CX-biotin nucleic acid labeling kit, by preliminarily diluting the solution with distilled water. pDNA was incubated for 60 min, and then biotin labeled pDNA was purified by ethanol precipitation. The concentration of biotin labeled pDNA was adjusted to 0.2 µg/µl (0.05 µM final), and then a 50 µl aliquot of the solution was incubated with a 10 µl aliquot of the QD-545 streptavidin (0.02 µM final concentration) in HEPES (pH 7.4) buffer at room temperature for at least 30 min. After QD labeling, the excess QD was purified from the labeled DNA by passing through the Sephadex G50 mini column, which is equilibrated with distilled water. FRET was optimized by partially replacing a 16DMAE-ss-PRX and 46DMAE-ss-PRX with rhodamine-DMAE-ss-PRX. The synthesis of rhodamine-DMAE-ss-PRX was described in Supplementary Data. Keeping a charge ratio constant at 5, fluorescence was measured in a real time fluorescence photometer (JASCO, FP-750 spectroflurometer, Tokyo, Japan), where the QDs were excited at 340 nm and an emission spectrum was collected from 550 to 650 nm.

### Confocal image studies

For confocal image studies $5 \times 10^4$ cells/well were seeded on 35-mm glass base dishes (IWAKI, Tokyo, Japan) for 2 days, and then transfected with T-MEND containing 0.4 µg of QD-labeled DNA condensed with acceptor-labeled DMAE-ss-PRX at 37°C under an atmosphere with 5% $CO_2$. At 3 h after transfection, medium was changed with fresh culture medium, and then incubated for additional 3 h. The nuclei were then stained with 1 µg/ml of Hoechst 33342, 15 min before observation. Cells were washed with 5 mM HEPES containing 20 U/ml of heparin sodium to remove the T-MEND bound on the cell-surface. Thereafter, medium was replaced with HEPES buffer (135 mM NaCl, 5.4 mM KCl, 1.0 mM $MgCl_2$, 1.8 mM $CaCl_2$, 5 mM HEPES and 10 mM glucose; pH = 7.3), and examined by confocal laser scanning microscopy (LSM 510 META; Carl Zeiss Co. Ltd, Jena, Germany) equipped with an oil-immersion objective lens (Plan-Apochromat 63×/NA = 1.4). Nucleus (Hoechst 33342) was excited by a 2-photon Maitai laser (780 nm). The QD was then excited by light (488 nm) from an argon laser. Imaging without the use of a UV laser is advantageous, in that it avoids cytotoxic effects of QD in response to the UV-radiation (19). The emitted light was filtered through a dichroic mirror (HFT488) and spectrophotometrically analyzed using a spectrophotometric detector (META) over a range of 530–630 nm in 10 nm increments. Spectral data are presented as relative fluorescence intensity compared to maximum intensity (545 nm).

For capturing the images by spectral mode (λ mode), the QD was similarly excited by light (488 nm) from an argon laser. The emitted light ranging from 537 to 569 nm, and >630 nm was simultaneously corrected by META equipment for the QD-and rhodamine-derived signals. These data were digitally exhibited in green (G) and red (R) channels, respectively. Thereafter, the Hoechst33342 signals excited by a 2-photon Maitai laser (780 nm) were captured, and digitally exhibited in blue (B) channel. The threshold for differentiating between heterochromatin and euchromatin was determined based on the histogram of the fluorescence intensity in each pixel ($x$-axis) versus the number of pixel areas ($y$-axis). In every region of interest (r.o.i) surrounding a total nucleus, the histogram represented a single-peaked spectrum at a lower level of fluorescence intensity. The pixels with higher intensities did not exhibit any peak, since distribution of intensity in each pixel is highly scattered. We denoted the highest tail of the single-peaked spectrum as a threshold fluorescent intensity to separate the heterochromatin and euchromatin regions.

### Quantification of pDNA by means of CIDIQ method

Intra-nuclear distribution and decondensation efficiency of plasmid DNA in intra-nuclear region was quantified by confocal image-assisted three-dimensionally integrated quantification (CIDIQ) method, which is originally developed to quantify the distribution of exogenous DNA in endosome/lysosome, cytosol, and nucleus with sequential Z-series images captured by confocal laser scanning microscopy (31). Z-series of images exported as 8-bit TIFF-format image data were transferred to an Image-Pro Plus software (Media Cybernetics Inc., Silver Spring, MD, USA). All of Z-series of stack files were

Downloaded from nar.oxfordjournals.org at (D) Hokkaido U Med on May 9, 2011

opened as merged file. Then it was allowed to measure pixel area count, which satisfy the threshold pixel intensity in each RGB images or arbitrary combination of RGB channels in marked region of interest (r.o.i.). Digital noise was filtered out by avoiding single-pixel signals. The counts in mock-treated cells (non-transfected cells) were negligible in the calculation of pixel areas in the G and R channels. Detail equation is listed in Supplementary Data.

To determine the minimal number of cells required for analysis, the statistical parameter of the coefficient of variation (C.V.) was determined. When the C.V. values for the fraction of pDNA in condensation and decondensation status in euchromatin and heterochromatin ($F^{hetero}{}_G$, $F^{hetero}{}_Y$, $F^{hetero}{}_R$, $F^{eu}{}_G$, $F^{eu}{}_Y$ and $F^{eu}{}_R$) were plotted against the number of the analyzed cells, all of the C.V. values reached a plateau at 10 cells (Supplementary Figure S1). Therefore, we concluded that 10 cells were sufficient to obtain reliable results.

## RESULTS

### Transgene expression transduced by T-MEND vector containing pcDNA3.1-luciferase

Since decondensation kinetics in cells and nucleus are altered depending on the pDNA condenser used (22), its selection is one of the key determining factors for gene expression efficiency. As the synthetic DNA condenser, we selected biocleavable polyrotaxane (DMAE-ss-PRX) in which cationic DMAE-α-CD units were linked together with poly (ethylene glycol) (PEG) chains (MW; 3500–4500) in monliform, and capped with disulfide-bonding (32,33) (Figure 1a). Two kinds of DMAE-ss-PRX were used in the present analysis, in which 16 or 46-dimethylaminoethyl (DMAE) units were incorporated in one molecule, in average. Here, we refer to as 16DMAE-ss-PRX and 46DMAE-ss-PRX, respectively. The core formed with 16DMAE-ss-PRX represented relatively higher size and polydispersity index (PDI) compared with 46DMAE-ss-PRX and protamine (Table 1).

To deliver the pDNA/polycation core to the nucleus, we used a T-MEND, the critical structural elements of which (23) are a DNA–polycation condensed core coated with two nuclear membrane-fusogenic inner envelopes and two endosome-fusogenic outer envelopes. It is designed to overcome the endosomal membrane and nuclear membranes via stepwise fusion, through a 'nuclear pore complex (NPC)-independent pathway' (Figure 1b). The resulting T-MEND particles formed with 16DMAE-ss-PRX had slightly larger diameters and PDI values compared with those prepared using 46DMAE-ss-PRX, but the *z*-potential was comparable for the two samples. The size of the T-MEND prepared with protamine was smaller, with a minimum PDI, and had a highly positive *z*-potential (Table 1). As shown in Figure 1c, the transfection activity of the T-MEND prepared with 46DMAE-ss-PRX showed a significantly higher gene expression compared with those prepared with 16DMAE-ss-PRX. The mock treated cells (non-transfected cells) showed negligible luciferase activity ($<10^3$ RLU/mg protein). Of note, the Z-potential of the T-MEND prepared with 46DMAE-ss-PRX was higher than a T-MEND prepared with protamine, a natural DNA condenser. Thus, the stimulated transfection activity of the T-MEND prepared with 46DMAE-ss-PRX cannot be explained by enhanced cellular uptake. As shown in Figure 1c, the transfection activity of T-MEND prepared with 46DMAE-ss-PRX represented significantly higher gene expression compared with those prepared with 16DMAE-ss-PRX. It is unique demonstration showing an impact of modulation of condenser on transfection activity of T-MEND (23). In the following experiments, we compared the intra-nuclear disposition of pDNA condensed with 16DMAE-ss-PRX and 46DMAE-ss-PRX.

**Table 1.** Dynamic light scattering studies of the core and R8 T-MEND, using Protamine, 16DMAE-ss-PRX and 46DMAE-ss-PRX with pcDNA 3.1-*luc*

| Name of packaging material | Size (nm) | Polydispersity index (PDI) | Zeta-potential (mV) |
|---|---|---|---|
| Core Protamine | 87–102 | 0.28–0.30 | (+) 27–30 |
| Core 16DMAE-ss-PRX | 135–150 | 0.24–0.37 | (+) 18–23 |
| Core 46DMAE-ss-PRX | 90–105 | 0.15–0.21 | (+) 22–28 |
| T-MEND (Protamine) | 150–189 | 0.15–0.20 | (+) 42–54 |
| T-MEND (16DMAE-ss-PRX) | 275–315 | 0.23–0.36 | (+) 25–33 |
| T-MEND (46DMAE-ss-PRX) | 200–221 | 0.15–0.19 | (+) 35–43 |

### Labeling of plasmid DNA and FRET optimization

For a labeling of pDNA with QD545, pDNA was first covalently labeled to biotin, followed by conjugation with streptavidin-modified QD. In this labeling, we incubated the QDs with biotin-labeled pDNA at a molar ratio of 0.4 (QD; 0.02 μM final and DNA; 0.05 μM final) to avoid a situation in which one pDNA possessed multiple numbers of QDs. If the reaction proceeds stoichiometrically, it would be expected that the pDNA would contain 0 or 1 QDs per pDNA molecule. After conjugation with the QDs, QD-labeled pDNA was purified on a Sephadex G50 mini column. Complete removal of free streptavidin-labeled QD was confirmed (Supplementary Figure S2). QD-labeling of DNA was validated by 1% agarose gel electrophoresis. As shown in Figure 2a, QD conjugated with pDNA (lane 'Pre') proceeded through the agarose gel more extensively compared with free QD (lane 'Q'). Free QDs are slightly charged molecules, the charge of which is derived from surface-modified streptavidin, while pDNA is highly negatively charged due to phosphate groups. Thus, QD, when conjugated with pDNA, developed extensively compared with free-form QDs by electrophoresis, although the size of the QDs is smaller than QD-conjugated pDNA. Moreover, the QD signals (Figure 2a; lane 'Pre') were overlapped to the pDNA signals which are appeared by staining with ethidium bromide (Figure 2b; lane 'Pre'). These findings also confirmed that QD-labeling did not occur in biotin-unlabeled pDNA (Supplementary Figure S2). Collectively, these

Downloaded from nar.oxfordjournals.org at (D) Hokkaido U Med on May 9, 2011

data indicate that QD-labeling can be achieved via specific avidin–biotin interactions. Compared with QD-unlabeled pDNA, bands corresponding to labeled pDNA (lanes 'Pre' and 'Pro') were broader, probably because the band includes QD-labeled and unlabeled pDNA, as described above. It is noteworthy that free form of QD was not detected after (lane 'Pro') and even before (lane 'Pre') the purification of QD-labeled pDNA. These data collectively suggested that QDs bound to the pDNA stoichiometrically.

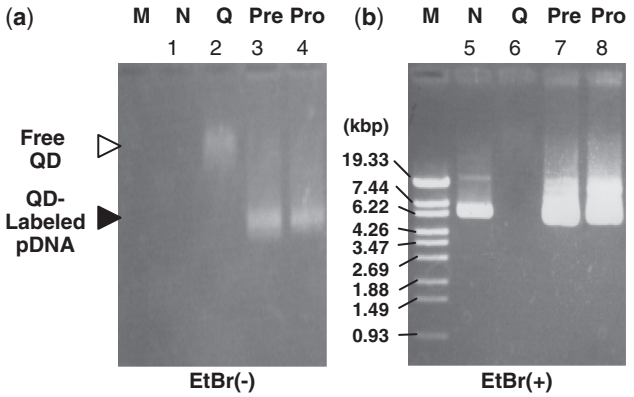



**Figure 2.** Confirmation of QD-labeling of pDNA by agarose gel electrophoresis. QD and pDNA was visualized by UV-irradiation before (**a**) and after (**b**) staining with EtBr. M, size marker; lanes 1 and 5, native pDNA; lanes 2 and 6, QD only; lanes 3 and 7, QD-labeled pDNA before purification; lanes 4 and 8, QD-labeled pDNA after purification. QD fluorescence was detected directly under UV irradiation without EtBr staining (a).

For FRET analysis, rhodamine-labeled PRXs were partially replaced with non-labeled DMAE-ss-PRX keeping a final $N/P$ ratio at 5 (Figure 3a). To minimize a change in the condensation/decondensation profile, same length of the PEG chain (MW; 3500–4500) was used. Each chain possessed one rhodamine unit in average. Acceptor-labeled polyrotaxane (Rho-DMAE-ss-PRX) was used as a portion of the condenser (5% of its weight in 16DMAE-ss-PRX and 46DMAE-ss-PRX). This confirms that the fluorescence of rhodamine labeled on DMAE-ss-PRX is not affected when it is subjected to condensation with QD (donor)-unlabeled pDNA, and excited at 543 nm, the optimum wave length for its excitation. Thus, the effect of self-quenching is negligible in this analysis. In both cases, partial replacement from DMAE-ss-PRX to Rho-DMAE-ss-PRX resulted in an increase of fluorescence intensity peaked at 590 nm by FRET, coupled with a decrease of fluorescence intensity peaked at 530 nm. The ratio of DMAE-ss-PRX to Rho-DMAE-ss-PRX was optimized where the signals at donor and acceptor were nearly equally detected (Figure 3b and c).

## Confocal imaging and CIDIQ analysis for quantification of pDNA

The cores, in which FRET occurred between QD545-labeled pDNA and rhodamine-labeled DMAE-ss-PRX were encapsulated to the T-MENDs, and then condensation/decondensation status in nucleus was evaluated using spectral imaging fluorescence microscopy. Typical spectral data with a core formed with 16DMAE-ss-PRX plus Rho-14DMAE-ss-PRX were represented in Figure 4

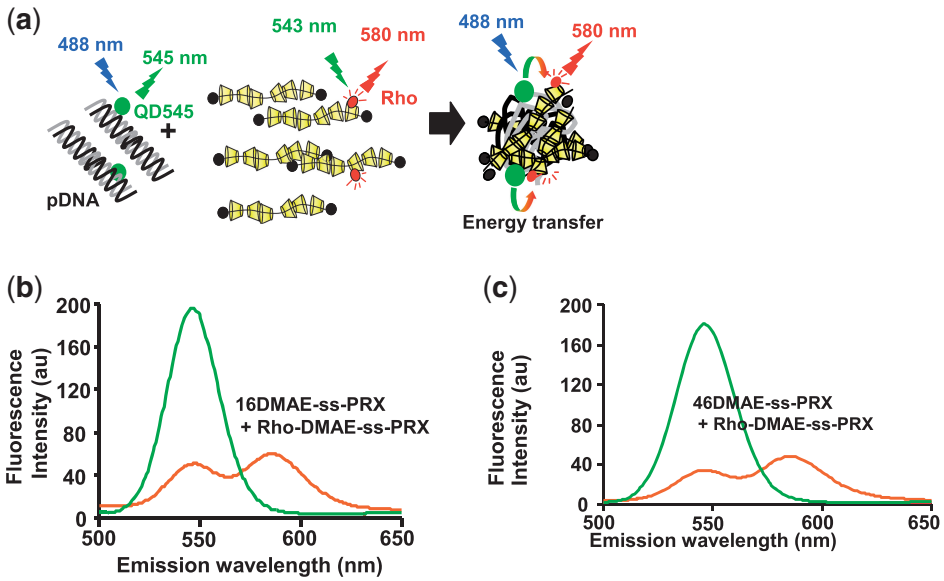



**Figure 3.** FRET between QD-labeled pDNA and rhodamine-labeled DMAE-ss-PRX. (**a**) Schematic diagram illustrating the principles of condensation-dependent FRET occurrence between QD-labeled pDNA and rhodamine-labeled DMAE-ss-PRX. (**b** and **c**) Optimized FRET between QD-labeled pDNA and rhodamine-labeled DMAE-ss-PRX. FRET between QD545 (excitation at 488 nm and emission at 545 nm) and rho-DMAE-ss-PRX was monitored by spectrophotometer. For condensation, QD-labeled pDNA was condensed with 16DMAE-ss-PRX containing Rho-DMAE-ss-PRX (b) and 46DMAE-ss-PRX containing Rho-DMAE-ss-PRX (c) keeping constant $N/P$ ratio at 5.

Downloaded from nar.oxfordjournals.org at (D) Hokkaido U Med on May 9, 2011

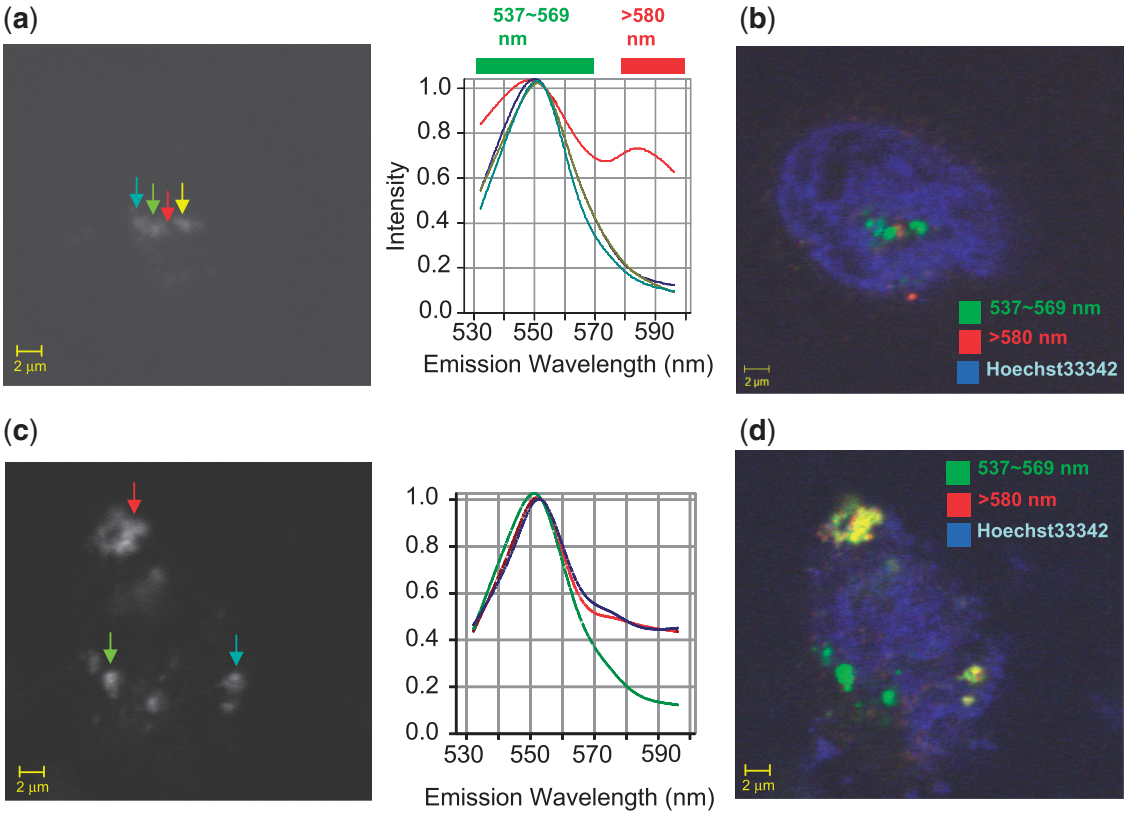



**Figure 4.** Optimization and intracellular visualization of FRET between QD-labeled pDNA and rhodamine-labeled DMAE-ss-PRX. (**a** and **c**) Typical spectra of clusters detected in nuclear region obtained after the transfection of T-MEND prepared with 16DMAE-ss-PRX plus rhodamine labeled DMAE-ss-PRX (a) or 46DMAE-ss-PRX plus rhodamine labeled DMAE-ss-PRX (c) as the relative fluorescence intensity compared to the maximum intensity observed at ~545 nm. (a) Blue, yellow and green arrows (left panel) and spectra lines (right panel) indicate the clusters, where FRET was completely cancelled (right panel). That indicated as red arrow and line represent cluster where FRET was partially cancelled. (c) Green arrow (left panel) and spectra line (right panel) indicate the clusters, where FRET was completely cancelled (right panel). Those indicated as red and blue arrows (left panel) and lines (right panel) represent cluster where FRET was partially cancelled. (**b** and **d**) Digital acquisition of QD- and rhodamine-derived signals. The emitted light derived from QD (ranging from 537 to 569 nm) and rhodamine (>580 nm) were corrected by META equipment, and then exhibited in green (G) and red (R) channels, respectively. Hoechst33342 signals excited by a 2-photon Maitai laser (780 nm) were captured, and digitally exhibited in blue (B) channel. (b and d) represent a results of 16DMAE-ss-PRX and 46DMAE-ss-PRX, respectively.

(Figure 4a for 16DMAE-ss-PRX and Figure 4c for 46DMAE-ss-PRX, respectively).

Some clusters represent single-peaked spectrum at 550 nm, which suggest the pDNA in completely decondensed form. Meanwhile, some clusters represent maximum peak at 590 nm as well as 550 nm, which represents pDNA in condensed form. Fluorescence ranging from 537 to 569 nm (donor fluorescence), and >580 nm (acceptor fluorescence) was separately collected by LSM510-META equipment, and then digitally exhibited in green (G) and red (R) channels, respectively (Figure 4b for 16DMAE-ss-PRX and Figure 4d for 46DMAE-ss-PRX, respectively). As described above, we conjugated pDNA with QDs using a molar ratio of 0.4 in this analysis. Thus, a fraction of the pDNA contains no QD labeling. However, this has no effect on the following data analysis, since pDNA, when free from donor (QD), does not emit fluorescence, either at 537–569 nm or at >580 nm. The nucleus was stained with Hoechst33342, and observed in a blue channel (B).

For the quantification of pDNA in condensed form and decondensed form, confocal image-assisted three-dimensionally integrated quantification (CIDIQ) method was used which are developed to quantify the intracellular distribution of pDNA (8,31,33). The boundaries of red and green clusters were first detected by digitally extracting the pixels above background levels (Figure 5a). The pixels appearing as green and red denoting pDNA in the decondensed form (Figure 5a-i), and the condensed form with (Figure 5a-ii) DMAE-ss-PRX, respectively. It is noteworthy that the pDNA detected in the cytoplasmic region (extra-nuclear regions) are mainly detected as red clusters (Supplementary Figure S3). Thus, pDNA exists in the condensed form in the cytoplasm, presumably because of the protection afforded by the lipid envelope. Pixels which satisfy red- and green-positive clusters are defined as yellow, which represents a partially decondensed pDNA (Figure 5a-iii). Yellow pixels are barely observed in 16DMAE-ss-PRX, whereas significant amounts of pixel areas were detected in 46DMAE-ss-PRX. Similarly, the intra-nuclear region was digitally divided into heterochromatin and euchromatin region by monitoring the fluorescence signals of Hoechst33342 (Figure 5a-iv). The other

Downloaded from nar.oxfordjournals.org at (D) Hokkaido U Med on May 9, 2011

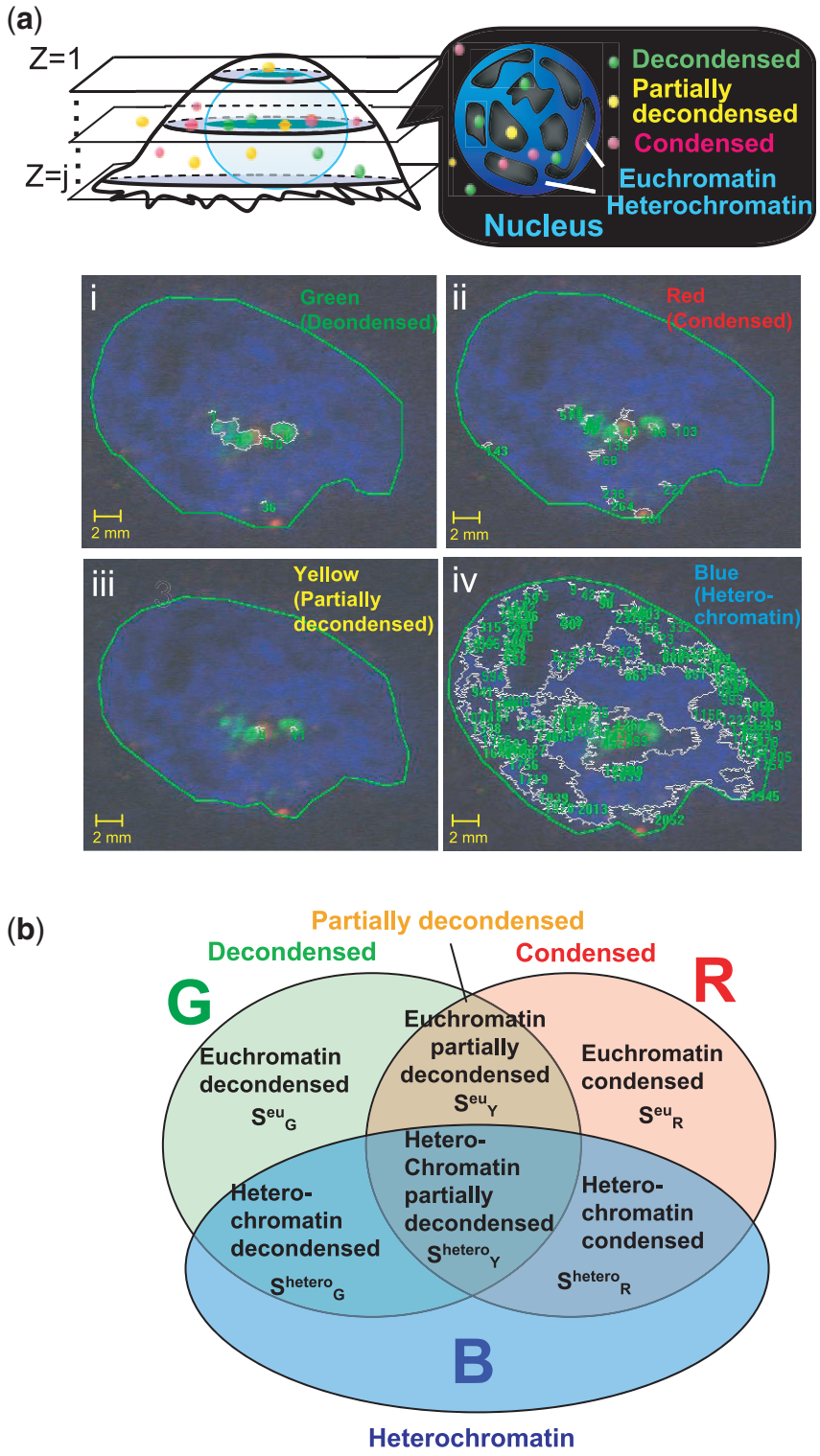



**Figure 5.** Schematic diagram illustrating the methodology to quantify the distribution and condensation/decondensation efficiency of pDNA. (**a**) A typical image showing the intracellular trafficking of pDNA transfected by a T-MEND prepared with 16DMAE-ss-PRX. Z-series of confocal images were captured by the LSM 510 META. The pixels exhibited as green, red and yellow clusters were exhibited as decondensed, condensed and partially decondensed pDNA. In addition, the heterochromatin region is defined as a region which possessed high fluorescence signals in B channel. Typical images representing a definition of clusters which have strong signals in G and R channels were shown in a(i), a(ii), in both G and R channels shown in a(iii) and in B channel shown in a(iv). (**b**) The pixel areas under the decondensed form, partially decondensed form and condensed form in heterochromatin and euchromatin region are separately integrated through all of the Z-series of confocal images, and then denoted as $S^{hetero}{}_k$ and $S^{hetero}{}_k$, respectively (Supplementary Equation), where $k$ is either R or Y or G.

Downloaded from nar.oxfordjournals.org at (D) Hokkaido U Med on May 9, 2011

intra-nuclear region was defined as the euchromatin region. Finally, the pixel areas of red, green and yellow clusters, in euchromatin and heterochromatin regions were independently integrated through all of the Z-series of confocal images, and denoted as $S^{eu}{}_k$ and $S^{hetero}{}_k$ (Figure 5b), where $k$ denote the G or R or Y.

First, pixel areas of pDNA in the whole nucleus were compared between 16DMAE-ss-PRX and 46DMAE-ss-PRX, which reflect a total nuclear delivery of pDNA. 46DMAE-ss-PRX represents higher nuclear delivery than that of 16DMAE-ss-PRX in average, which may partially contribute to the higher gene expression (Figure 6a). Subsequently, fraction of pDNA under condensed, partially decondensed and decondensed pDNA was compared in the whole nucleus (Figure 6b). In 16DMAE-ss-PRX, nearly equal fraction of pDNA exists as decondensed and condensed form (~50% in average). Partially decondensed pDNA represents very little contribution in total nuclear pDNA. In contrast, in 46DMAE-ss-PRX, decondensed pDNA mainly sheared the pDNA in the whole nucleus (>70% in average). Of note, partially decondensed pDNA contributed a significant part (~12% in average) of pDNA, which is one of the significant characters different form 16DMAE-ss-PRX. The total pixel areas of pDNA as decondensed form in whole nucleus were plotted in Figure 6c, which is an index for the nuclear amount of pDNA in decondensed form. The higher value (~4-fold) in 46DMAE-ss-PRX is in good agreement with the significantly higher gene expression in 46DMAE-ss-PRX (Figure 1c).

To provide an insight into the difference in disposition of pDNA between 16DMAE-ss-PRX and 46DMAE-ss-PRX, condensation/decondensation conditions in euchromatin and heterochromatin regions were independently evaluated. As shown in Figure 7a, a considerable amount of pDNA was distributed to the heterochromatin and euchromatin regions in 16DMAE-ss-PRX (~60 and 40%, respectively; black circle, Supplementary Table S1). However, the condensation/decondensation status of pDNA was completely different in heterochromatin and euchromatin. In heterochromatin, the pDNA was mainly present as the decondensed form, and *vice versa* in euchromatin (Supplementary Table S1). As a result, decondensation efficiency in heterochromatin ($E^{hetero}$) is drastically higher than that in euchromatin ($E^{eu}$) (~70 and 25% in average, respectively; Figure 7d). On the other hand, in 46DMAE-ss-PRX, >70% of pDNA was distributed to euchromatin region in average (Figure 7b; black circle). Moreover, the most unique character in 46DMAE-ss-PRX is that major part of pDNA (>70%) exists as a decondensed form in euchromatin region (Figure 7b and e). It should be noted here that neither labeling DNA with QD, nor a polycation with rhodamine, affects the size and zeta-potentials of particles (Supplementary Table S2).

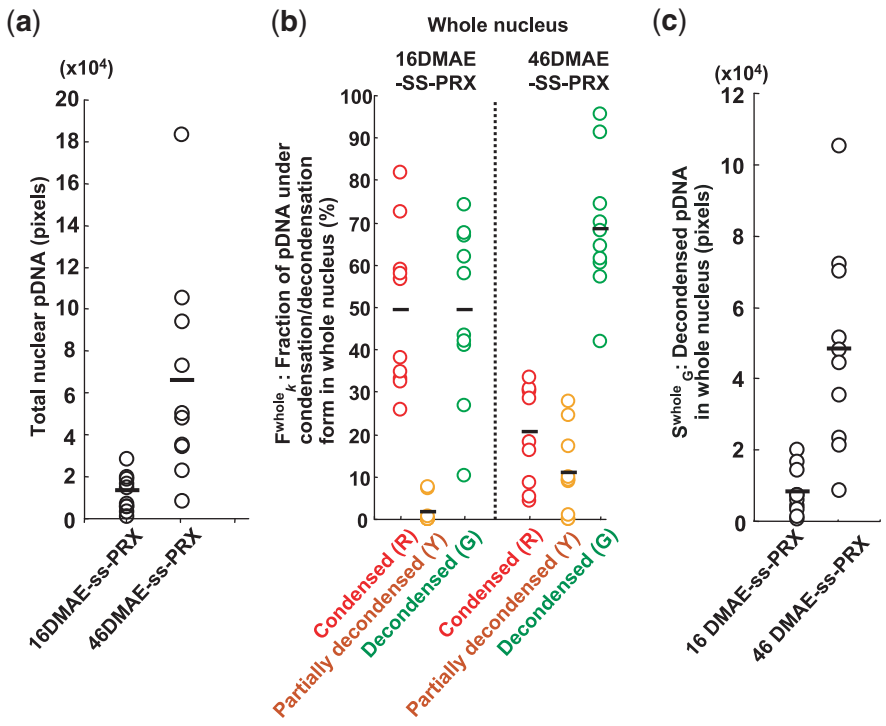



**Figure 6.** Quantification of p-DNA status in whole nucleus. (**a**) The total pixel area of pDNA calculated as ($S^{whole}{}_G, + S^{whole}{}_R + S^{whole}{}_Y$), which is an index of the total accumulation of pDNA in the whole nucleus plotted. (**b**) Fraction of pDNA in condensed-, decondensed- and partially decondensed form in whole nucleus. $F^{whole}{}_k$ values were calculated as described in 'Materials and Methods' section, where $k$ is R, G and Y, respectively. (**c**) Total pixel areas of decondensed pDNA in whole nucleus. Total pixel area of pDNA observed as decondensed form in whole nucleus was calculated as described in 'Materials and Methods' section, and plotted. Circles and bars represent calculated values in independent 10 cells and mean values.

Downloaded from nar.oxfordjournals.org at (D) Hokkaido U Med on May 9, 2011

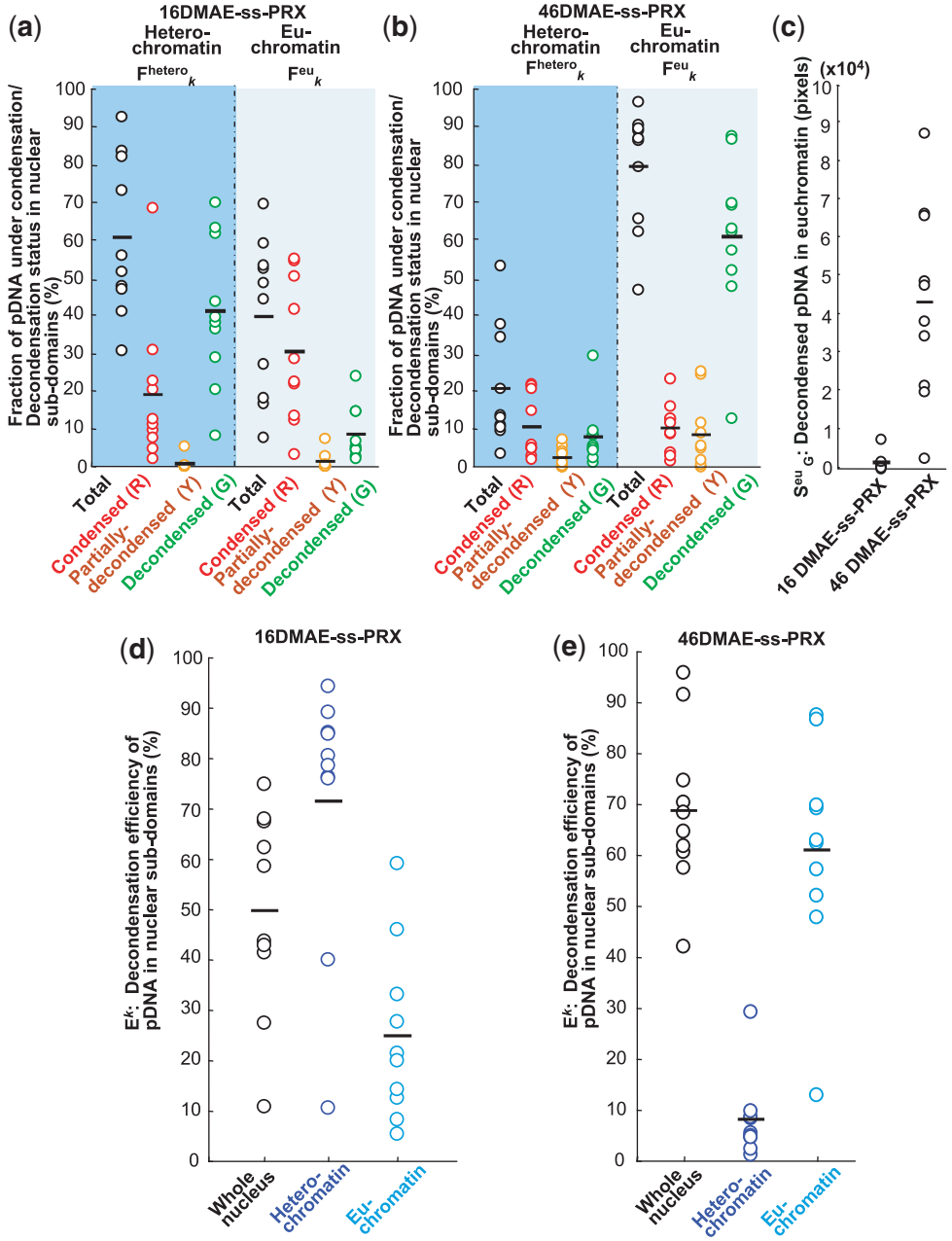



**Figure 7.** Procedures for quantification of pDNA under condensed/decondensed form in intra-nuclear subdomains. (**a** and **b**) Fraction of pDNA in condensed-, decondensed- and partially decondensed form in nuclear subdomains. $F^{hetero}{}_k$ and $F^{eu}{}_k$ values were determined as described in 'Materials and Methods' section after the transfection with 16DMAE-ss-PRX (a) and 46DMAE-ss-PRX (b), where $k$ is R, G and Y, respectively. (**c**) Total pixel areas of decondensed pDNA in euchromatin region. $S^{eu}{}_G$ values were calculated as described in 'Materials and Methods' section, and plotted. Circles and bars represent calculated values in independent 10 cells and mean values. After the transfection with T-MENDs prepared with 16DMAE-ss-PRX (**d**) and 46DMAE-ss-PRX (**e**), decondensation efficiencies of pDNA in whole nucleus ($E^{whole}$), heterochromatin ($E^{hetero}$) and euchromatin ($E^{eu}$) were plotted. Formulas for calculation of $E^{whole}$, $E^{hetero}$ and $E^{eu}$ were described in Supplementary Data.

## DISCUSSION

In the present study, we established a method for quantifying the intra-nuclear localization and condensation/decondensation status of pDNA from a condenser in the nucleus. We imaged the intra-nuclear FRET, occurring from donor (QD)-labeled pDNA and acceptor (rhodamine)-labeled DMAE-ss-PRX. Thus, the definition of FRET-cancelled signals (green) is the pDNA released from DMAE-ss-PRX, but it includes pDNA condensed with other intra-nuclear components. Using this technique, we found that modulation of the supra-molecular structure of polyrotaxane affects intra-nuclear disposition. In our study, we evaluated intra-nuclear disposition at 3 h post-transfection, while transient transgene expression was examined at 24 h post-transfection. Since the metabolic stability of pDNA by DNase digestion is short (half-life; <1–2 h) (34), we assume that the initial-phase of intracellular trafficking and intra-nuclear disposition accurately

Downloaded from nar.oxfordjournals.org at (D) Hokkaido U Med on May 9, 2011

reflect the transfection activity. The most striking difference between 16DMAE-ss-PRX and 46DMAE-ss-PRX is that pDNA cores formed with 16DMAE-ss-PRX were dominantly decondensed from polycation in heterochromatin region (Figure 7a and d), while those prepared with 46DMAE-ss-PRX were preferentially decondensed in euchromatin region (Figure 7b and e).

Since we previously reported that the cleavage of SS bonds in the capping structure by dithiothreitol is not sufficient for decondensation (35), tentative swelling and opening-up of the particle structure is not likely. We previously found that the nuclear transcription efficiency of lipoplex in terms of the ratio of gene expression-positive cells to nuclear pDNA-positive cells drastically increased in the late S and G2/M phase (36), when histone mRNA increases. Replacement with a cationic counterpart such as a histone might be a possible driving force for decondensation in DMAE-ss-PRX. Taking the mechanism for the nuclear delivery by a T-MEND into the consideration, the difference in nuclear region-dependent decondensation properties can be explained by the nuclear structure and the degree of resistance to decondensation in a cationic histone-rich environment. Histological electron microscopic observations of the nucleus clarified that the nuclear lamina meshwork plays an important role in controlling nuclear shape, and that a subset of heterochromatin is located against the inner surface of the lamina. As a result, heterochromatin forms a rim around the nucleus and is interrupted by nuclear pores (37). Therefore, it is plausible that the nascent polyplexes, introduced by nuclear membrane fusion first pass through the histone-rich heterochromatin region. Since 16DMAE-ss-PRX has less cationic DMAE units in one chain compared to 46DMAE-ss-PRX, it may form a looser complex. It is supported by the fact that pDNA core formed with 16DMAE-ss-PRX are larger in size, compared to that prepared with 46DMAE-ss-PRX (Table 1 and Supplementary Table S2). Thus, decondensation of pDNA from 16DMAE-ss-PRX may be extensively triggered in heterochromatin by replacement of counterpart from cationic polymer to basic histone, enriched in the heterochromatin region. In contrast, pDNA forms more tightly condensed particle with 46DMAE-ss-PRX. Therefore, it may be resistant to the undesired decondensation in heterochromatin region. It remains to be clarified a driving force of the efficient euchromatic decondensation in 46DMAE-ss-PRX. Euchromatin decondensation was subsequently accelerated by the natural cellular dynamics of transcriptions so that the higher green pixel area was found, which was consistent with the respective transfection activities (Figures 1c and 7c).

Meanwhile, the issue of whether heterochromatin/euchromatin localization extends to the next-generation cell is an important issue to be clarified, since it is closely linked to the sustained gene expression. However, the intra-nuclear behavior of pDNA during cell-division is not completely understood. While some reports showed that fluorescence-tagged pDNA is excluded from daughter cells (38), another report showed that pDNAs tagged with protein nucleic acid (PNA) are evenly separated between next-generation cells (39). The question is whether pDNA transfected by a non-viral vector behaves as chromosomal DNA or extra-chromosomal DNA remains to be clarified in the future. The T-MEND was originally developed for use as a gene carrier for dendritic cells (23). The control of intra-nuclear disposition may offer more efficient antigen-expression and presentation in dendritic cells and could be the basis for practical use in DNA vaccination thereby.

In conclusion, we developed a *de novo* method for quantifying the decondensation of pDNA in heterochromatin and euchromatin separately by means of a QD-FRET technique. Using this system, the findings show that the condensation/decondensation efficacy in heterochromatin and euchromatin can be successfully controlled by modulating the number of cationic moieties per molecule of DMAE-ss-PRX, so that a therapeutic gene can be efficiently delivered to the euchromatin sub-domain. QD-FRET imaging technology is highly advantageous for clarifying the dynamics of plasmid DNA in post-nuclear delivery processes.

## SUPPLEMENTARY DATA

Supplementary Data are available at NAR Online.

## ACKNOWLEDGEMENTS

The authors thank Mr Junpei Horiuchi, Japan Advanced Institute of Science and Technology, for his cooperation in preparing Rho-DMAE-ss-PRX; and Dr Milton S. Feather for his helpful advice in writing the English article.

## FUNDING

Special Coordination Funds for Promoting Science and Technology, and in part by a Grant-in-Aid for Scientific Research (S) and Young Scientists (A) from the Ministry of Education, Culture, Sports, Science and Technology (MEXT) of Japan. Funding for open access charge: Grant-in-Aid for Grant-in-Aid for Scientific Research (S) from the Ministry of Education, Culture, Sports, Science and Technology (MEXT) of Japan.

*Conflict of interest statement*. None declared.

## REFERENCES

1. Mastrobattista,E., van der Aa,M.A., Hennink,W.E. and Crommelin,D.J. (2006) Artificial viruses: a nanotechnological approach to gene delivery. *Nat. Rev. Drug Discov.*, **5**, 115–121.
2. Rice,J., Ottensmeier,C.H. and Stevenson,F.K. (2008) DNA vaccines: precision tools for activating effective immunity against cancer. *Nat. Rev. Cancer*, **8**, 108–120.
3. Rossi,J.J., June,C.H. and Kohn,D.B. (2007) Genetic therapies against HIV. *Nat. Biotechnol.*, **25**, 1444–1454.
4. Hacein-Bey-Abina,S., Kalle,C.v., Schmidt,M., Deist,L.F., Wulffraat,N., McIntyre,E., Radford,I., Villeval,J.-L., Fraser,C.C., Cavazzana-Calvo,M. *et al.* (2003) A serious adverse event after successful gene therapy for X-linked severe combined immunodeficiency. *N. Engl. J. Med.*, **348**, 255–256.
5. Marshall,E. (1999) Gene therapy death prompts review of adenovirus vector. *Science*, **286**, 2244–2245.

Downloaded from nar.oxfordjournals.org at (D) Hokkaido U Med on May 9, 2011

6. Kamiya,H., Akita,H. and Harashima,H. (2003) Pharmacokinetic and pharmacodynamic considerations in gene therapy. *Drug Discov. Today*, **8**, 990–996.
7. Hama,S., Akita,H., Iida,S., Mizuguchi,H. and Harashima,H. (2007) Quantitative and mechanism-based investigation of post-nuclear delivery events between adenovirus and lipoplex. *Nucleic Acids Res.*, **35**, 1533–1543.
8. Hama,S., Akita,H., Ito,R., Mizuguchi,H., Hayakawa,T. and Harashima,H. (2006) Quantitative comparison of intracellular trafficking and nuclear transcription between adenoviral and lipoplex systems. *Mol. Ther.*, **13**, 786–794.
9. Varga,C.M., Tedford,N.C., Thomas,M., Klibanov,A.M., Griffith,L.G. and Lauffenburger,D.A. (2005) Quantitative comparison of polyethylenimine formulations and adenoviral vectors in terms of intracellular gene delivery processes. *Gene Ther.*, **12**, 1023–1032.
10. Gasser,S.M. (2002) Visualizing chromatin dynamics in interphase nuclei. *Science*, **296**, 1412–1416.
11. Reuter,G. and Spierer,P. (1992) Position effect variegation and chromatin proteins. *Bioessays*, **14**, 605–612.
12. Spector,D.L. (2001) Nuclear domains. *J. Cell Sci.*, **114(Pt 16)**, 2891–2893.
13. Stein,G.S., Zaidi,S.K., Braastad,C.D., Montecino,M., van Wijnen,A.J., Choi,J.Y., Stein,J.L., Lian,J.B. and Javed,A. (2003) Functional architecture of the nucleus: organizing the regulatory machinery for gene expression, replication and repair. *Trends Cell Biol.*, **13**, 584–592.
14. Breuzard,G., Tertil,M., Gonçalves,C., Cheradame,H., Géguan,P., Pichon,C. and Midoux,P. (2008) Nuclear delivery of NF$\kappa$B-assisted DNA/Polymer complexes: plasmid DNA quantification by confocal laser scanning microscopy and evidence of nuclear polyplexes by FRET imaging. *Nucleic Acid Res.*, **36**, e71.
15. Itaka,K., Harada,A., Yamasaki,Y., Nakamura,K., Kawaguchi,H. and Kataoka,K. (2004) In situ single cell observation by fluorescence resonance energy transfer reveals fast intra-cytoplasmic delivery and easy release of plasmid DNA complexed with linear polyethylenimine. *J. Gene Med.*, **6**, 76–84.
16. Madeira,C., Loura,L.M., Aires-Barros,M.R., Fedorov,A. and Prieto,M. (2003) Characterization of DNA/lipid complexes by fluorescence resonance energy transfer. *Biophys J.*, **85**, 3106–3119.
17. Medintz,I.L., Uyeda,H.T., Goldman,E.R. and Mattoussi,H. (2005) Quantum dot bioconjugates for imaging, labelling and sensing. *Nat. Mater.*, **4**, 435–446.
18. Srinivasan,C., Lee,J., Papadimitrakopoulos,F., Silbart,L.K., Zhao,M. and Burgess,D.J. (2006) Labeling and intracellular tracking of functionally active plasmid DNA with semiconductor quantum dots. *Mol. Ther.*, **14**, 192–201.
19. Derfus,A.M., Chan,W.C.W. and Bhatia,S.N. (2004) Probing the cytotoxicity of semiconductor quantum dots. *Nano Lett.*, **4**, 11–18.
20. Chen,F.Q. and Gerion,D. (2004) Fluorescent CdSe/ZnS nanocrystal-peptide conjugates for long-term, nontoxic imaging and nuclear targeting in living cells. *Nano Lett.*, **4**, 1827–1832.
21. Algar,W.R. and Krull,U.J. (2008) Quantum dots as donors in fluorescence resonance energy transfer for the bioanalysis of nucleic acids, proteins, and other biological molecules. *Anal. Bioanal. Chem.*, **391**, 1609–1618.
22. Chen,H.H., Ho,Y.P., Jiang,X., Mao,H.Q., Wang,T.H. and Leong,K.W. (2008) Quantitative comparison of intracellular unpacking kinetics of polyplexes by a model constructed from quantum dot-FRET. *Mol. Ther.*, **16**, 324–332.
23. Akita,H., Kudo,A., Minoura,A., Yamaguti,M., Khalil,I.A., Moriguchi,R., Masuda,T., Danev,R., Nagayama,K., Kogure,K. *et al.* (2009) Multi-layered nanoparticles for penetrating the endosome and nuclear membrane via a step-wise membrane fusion process. *Biomaterials*, **30**, 2940–2949.
24. Yui,N. and Ooya,T. (2006) Molecular mobility interlocked structures exploiting new functions of advanced biomaterials. *Cem. Eur. J.*, **12**, 6730–6737.
25. Futaki,S., Ohashi,W., Suzuki,T., Niwa,M., Tanaka,S., Ueda,K., Harashima,H. and Sugiura,Y. (2001) Stearylated arginine-rich peptides: a new class of transfection systems. *Bioconjug. Chem.*, **12**, 1005–1011.
26. Kakudo,T., Chaki,S., Futaki,S., Nakase,I., Akaji,K., Kawakami,T., Maruyama,K., Kamiya,H. and Harashima,H. (2004) Transferrin-modified liposomes equipped with a pH-sensitive fusogenic peptide: an artificial viral-like delivery system. *Biochemistry*, **43**, 5618–5628.
27. Masuda,T., Akita,H. and Harashima,H. (2005) Evaluation of nuclear transfer and transcription of plasmid DNA condensed with protamine by microinjection: the use of a nuclear transfer score. *FEBS Lett.*, **579**, 2143–2148.
28. Kogure,K., Moriguchi,R., Sasaki,K., Ueno,M., Futaki,S. and Harashima,H. (2004) Development of a non-viral multifunctional envelope-type nano device by a novel lipid film hydration method. *J. Control Release*, **98**, 317–323.
29. Lee,R.J. and Huang,L. (1996) Folate-targeted, anionic liposome-entrapped polylysine-condensed DNA for tumor cell-specific gene transfer. *J. Biol. Chem.*, **271**, 8481–8487.
30. Kaul,Z., Yaguchi,T., Harada,J.I., Ikeda,Y., Hirano,T., Chiura,H.X., Kaul,S.C. and Wadhwa,R. (2007) An antibody-conjugated internalizing quantum dot suitable for long-term live imaging of cells. *Biochem. Cell Biol.*, **85**, 133–140.
31. Akita,H., Ito,R., Khalil,I.A., Futaki,S. and Harashima,H. (2004) Quantitative three-dimensional analysis of the intracellular trafficking of plasmid DNA transfected by a nonviral gene delivery system using confocal laser scanning microscopy. *Mol. Ther.*, **9**, 443–451.
32. Ooya,T., Choi,H.S., Yamashita,A., Yui,N., Sugaya,Y., Kano,A., Maruyama,A., Akita,H., Ito,R., Kogure,K. *et al.* (2006) Biocleavable polyrotaxane-plasmid DNA polyplex for enhanced gene delivery. *J. Am. Chem. Soc.*, **128**, 3852–3853.
33. Yamashita,A., Yui,N., Ooya,T., Kano,A., Maruyama,A., Akita,H., Kogure,K. and Harashima,H. (2006) Synthesis of a biocleavable polyrotaxane-plasmid DNA (pDNA) polyplex and its use for the rapid nonviral delivery of pDNA to cell nuclei. *Nat. Protoc.*, **1**, 2861–2869.
34. Lechardeur,D., Sohn,K.J., Haardt,M., Joshi,P.B., Monck,M., Graham,R.W., Beatty,B., Squire,J., O'Brodovich,H. and Lukacs,G.L. (1999) Metabolic instability of plasmid DNA in the cytosol: A potential barrier to gene transfer. *Gene Ther.*, **6**, 482–497.
35. Yamada,Y., Nomura,T., Harashima,H., Yamashita,A., Katoono,R. and Yui,N. (2010) Intranuclear DNA release is a determinant of transfection activity for a non-viral vector: biocleavable polyrotaxane as a supramolecularly dissociative condenser for efficient intranuclear DNA release. *Biol. Pharm. Bull.*, **33**, 1218–1222.
36. Akita,H., Ito,R., Kamiya,H., Kogure,K. and Harashima,H. (2007) Cell cycle dependent transcription, a determinant factor of heterogeneity in cationic lipid-mediated transgene expression. *J. Gene Med.*, **9**, 197–207.
37. Weiss,L. (1989) The cell (Chapter 1). In Weiss,L. (ed.), *Cell and Tissue Biology - A Textbook of Histology*, 6th edn. Urban & Schwarzenberg Inc., Baltimore, pp. 1–65.
38. Ludtke,J.J., Sebestyen,M.G. and Wolff,J.A. (2002) The effect of cell division on the cellular dynamics of microinjected DNA and dextran. *Mol. Ther.*, **5**, 579–588.
39. Gasiorowski,J. and Dean,D.A. (2005) Postmitotic nuclear retention of episomal plasmids is altered by DNA labeling and detection methods. *Mol. Ther.*, **12**, 460–467.
40. Khalil,I.A., Kogure,K., Futaki,S. and Harashima,H. (2006) High density of octaarginine stimulates macropinocytosis leading to efficient intracellular trafficking for gene expression. *J. Biol. Chem.*, **281**, 3544–3551.


Downloaded from nar.oxfordjournals.org at (D) Hokkaido U Med on May 9, 2011